

Central Lancashire Online Knowledge (CLoK)

Title	Optimised solution-phase synthesis of NanoMIPs for protein detection in electrochemical diagnostics
Type	Article
URL	https://clock.uclan.ac.uk/54538/
DOI	https://doi.org/10.1088/1748-605X/adb672
Date	2025
Citation	Stephen, Andrei Nino, Holden, Mark, Sullivan, Mark Vincent, Turner, Nicholas W, Dennison, Sarah Rachel and Reddy, Subrayal M orcid iconORCID: 0000-0002-7362-184X (2025) Optimised solution-phase synthesis of NanoMIPs for protein detection in electrochemical diagnostics. Biomedical Materials. ISSN 1748-6041
Creators	Stephen, Andrei Nino, Holden, Mark, Sullivan, Mark Vincent, Turner, Nicholas W, Dennison, Sarah Rachel and Reddy, Subrayal M

It is advisable to refer to the publisher's version if you intend to cite from the work.
<https://doi.org/10.1088/1748-605X/adb672>

For information about Research at UCLan please go to <http://www.uclan.ac.uk/research/>

All outputs in CLoK are protected by Intellectual Property Rights law, including Copyright law. Copyright, IPR and Moral Rights for the works on this site are retained by the individual authors and/or other copyright owners. Terms and conditions for use of this material are defined in the <http://clock.uclan.ac.uk/policies/>

ACCEPTED MANUSCRIPT • OPEN ACCESS

Optimised solution-phase synthesis of NanoMIPs for protein detection in electrochemical diagnostics

To cite this article before publication: Andrei N Stephen *et al* 2025 *Biomed. Mater.* in press <https://doi.org/10.1088/1748-605X/adb672>

Manuscript version: Accepted Manuscript

Accepted Manuscript is “the version of the article accepted for publication including all changes made as a result of the peer review process, and which may also include the addition to the article by IOP Publishing of a header, an article ID, a cover sheet and/or an ‘Accepted Manuscript’ watermark, but excluding any other editing, typesetting or other changes made by IOP Publishing and/or its licensors”

This Accepted Manuscript is © 2025 The Author(s). Published by IOP Publishing Ltd.



As the Version of Record of this article is going to be / has been published on a gold open access basis under a CC BY 4.0 licence, this Accepted Manuscript is available for reuse under a CC BY 4.0 licence immediately.

Everyone is permitted to use all or part of the original content in this article, provided that they adhere to all the terms of the licence <https://creativecommons.org/licenses/by/4.0>

Although reasonable endeavours have been taken to obtain all necessary permissions from third parties to include their copyrighted content within this article, their full citation and copyright line may not be present in this Accepted Manuscript version. Before using any content from this article, please refer to the Version of Record on IOPscience once published for full citation and copyright details, as permissions may be required. All third party content is fully copyright protected and is not published on a gold open access basis under a CC BY licence, unless that is specifically stated in the figure caption in the Version of Record.

View the [article online](#) for updates and enhancements.

Optimised Solution-Phase Synthesis of NanoMIPs for Protein Detection in Electrochemical Diagnostics

AN Stephen¹, MA Holden¹ MV Sullivan^{2,3}, NW Turner², SR Dennison¹ and SM Reddy^{1*}

¹Department of Chemistry, Institute of Materials and Investigative Sciences, UCLan Centre for Smart Materials, School of Pharmacy and Biomedical Sciences, University of Central Lancashire, Preston, PR1 2HE, UK; ²Department of Chemistry, University of Sheffield, Dainton Building, 13 Brook Hill, Sheffield, S3 7HF; ³Micro/Bio/Nanofluidics Unit, Okinawa Institute of Science and Technology Graduate University, 1919-1 Tancha, Onna-son, Okinawa, 904-0495, Japan.

*Corresponding author: smreddy@uclan.ac.uk

Abstract

NanoMIPs are nanoscale molecularly imprinted polymers (MIPs) ranging in size between 30 to 300 nm offering a high affinity binding reagent as an alternative to antibodies. They are being extensively researched for applications in biological extraction, disease diagnostics and biosensors. Various methodologies for nanoMIP production have been reported demonstrating variable timescales required, sustainability, ease of synthesis and final yields. We report herein a fast (< 1hr) method for one pot aqueous phase synthesis of nanoMIPs using an acrylamide-based monomer and N,N'-methylenebisacrylamide crosslinker. NanoMIPs were produced for a model protein template namely haemoglobin from bovine species. We demonstrate that nanoMIPs can be produced within 15 minutes. We investigated reaction quenching times between 5 and 20 minutes. Dynamic light scattering results demonstrate a distribution of particle sizes (30 nm to 900 nm) depending on reaction termination time, with hydrodynamic particle diameter increasing with increasing reaction time. We attribute this to not only particle growth due to polymer chain growth but based on AFM analysis, also a tendency (after reaction termination) for particles to agglomerate at longer reaction times. Batches of nanoMIPs ranging 400 to 800 nm, 200 to 400 nm and 100 to 200 nm were isolated using membrane filtration. The batches were captured serially on decreasing pore size microporous polycarbonate membranes (800 to 100 nm) and then released with sonication to isolate nanoMIP batches in the aforementioned ranges. Rebinding affinities of each batch were determined using electrochemical impedance spectroscopy, by first trapping nanoMIP particles within an electropolymerized thin layer. Binding constants determined for NanoMIPs using the E-MIP sensor approach are in good agreement with surface plasmon resonance results. We offer a rapid (<2 hr) and scalable method for the mass production (40-80 mg per batch) of high affinity nanoMIPs.

Keywords

molecularly imprinted polymers; nanoMIPs; affinity reagents; protein diagnostics; electrochemical

1
2
3 41
4
5 42
6
7 43
8 44
9
10 45
11 46
12 47
13 48
14 49
15 50
16 51
17 52
18 53
19 54
20 55
21 56
22 57
23 58
24 59
25 60
26 61
27 62
28 63
29 64
30 65
31
32
33
34
35
36
37
38
39
40
41
42
43
44
45
46
47
48
49
50
51
52
53
54
55
56
57
58
59
60

Highlights

- **Rapid, high-yield synthesis of nanoMIPs:** Scalable production of high-affinity nanoMIPs achieved within 1 hour, yielding 40–80 mg per 20 mL batch.
- **Hydrodynamic size-driven separation:** A simple and reproducible process for purifying nanoMIPs based on particle diameter.
- **Electrochemical detection of proteins:** NanoMIPs successfully employed in electrochemical biosensors as antibody substitutes for selective protein recognition.

1. Introduction

The immunodiagnostic sector constitutes a multi-billion-dollar industry[1], heavily reliant on the widespread availability and utilization of animal-derived monoclonal and/or polyclonal antibodies. Within this sector, there exists a significant demand for reliable synthetic receptor technologies capable of mimicking antibody binding affinities, particularly in detecting protein and viral biomarkers especially when antibodies are unreliable or are difficult to produce. Technologies, with the potential to replace traditional antibodies in disease diagnostics, bio-extraction and purification, include molecularly imprinted polymers (MIPs), which represent a rapidly evolving class of synthetic antigen-recognition materials. MIPs feature cavities or binding sites capable of selectively re-binding specific biomolecules like protein antigens or viruses, offering an alternative to antibodies that is synthetically produced, stable, ethically sound, and cost-effective.

Acrylamide-based polymer hydrogels, extensively researched for their protein-selective properties, serve as a prominent example of MIPs. These hydrogels, produced using inexpensive reagents, can be synthesized in a single day through a one-pot process, resulting in micron-sized particles [2-5], thin films [6-9], and nanoscale particles [10-12] ranging from 50 to 200 nanometres. Our recent advances include the development of virus-imprinted MIPs for selectively capturing and neutralizing animal viruses [13]. Additionally, a MIP-based electrochemical sensor strategy has been demonstrated for the antibody-free determination of SARS-CoV-2 in saliva [14], with electrochemically produced MIPs showing promise for the detection of proteins at sub-nanomolar levels [15].

MIPs have been synthesised through various methods, involving either chemical or electrochemical initiation[15-17], resulting in suspensions of micro and/or nanoparticles in gel form within solutions[11, 18, 19] or as thin films[20-22]. IR spectroscopy of polyacrylamide-based MIPs have been previously reported showing the presence of amide functional groups[20] It was also demonstrated in the same publication that hydrogen bonding interactions can occur between target protein and potential MIP binding sites. Traditionally, MIP synthesis has involved creating a monolith (bulk) MIP using acryloyl-based monomers like acrylamide [18], acrylic acid, and N-hydroxymethylacrylamide (NHMA) [8], leading to the formation of polymeric hydrogels. The polymer gel monolith is then mechanically broken down via manual sieving or grinding to generate micron-sized particles, exposing target-specific cavities on each particle's surface. However, due to the rudimentary nature of the grinding process, there is limited control over the physical characteristics of the final particles, resulting in the creation of random nanoscale features alongside the desired cavities. Consequently, MIPs produced in this manner exhibit minimal homogeneity and are susceptible to nonspecific binding, leading to lower binding affinities for the target.

Recent approaches have focused on the formation of nanoscale MIPs (nanoMIPs) on a solid phase employing a bottom-up methodology to create MIP particles that closely resemble the target in dimension [11, 19, 23-26]. This results in MIPs with higher affinity, as the binding sites exhibit a 'one-to-one' correspondence with the target protein. Two synthesis methods have been extensively explored solid phase support synthesis and solution phase. With solid

1
2
3 107 phase support, micrometre sized glass beads have been the favoured substrate [11]. The
4 108 template molecule is chemically immobilised to glass beads which are then packed in a
5 109 column. A reaction mixture consisting of functional monomers, crosslinker and initiators are
6 110 then flowed through the column with subsequent nanoMIP growth occurring at the template-
7 111 functionalised glass beads. After reaction quenching [11], the nanoMIPs selectively bound to
8 112 the glass beads are released into solution and harvested using extended dialysis and
9 113 lyophilisation. This a multi-step process taking at least 3 days to produce 18 mg of material.
10 114 Albeit low yields, the method produces monodisperse particles with high affinity for target
11 115 template. The solution phase microgel method involves precipitation polymerisation where a
12 116 very dilute polymer solution, the template and the crosslinker in solution is used. This
13 117 polymerisation technique starts like the bulk monolith method however, it is stopped just
14 118 before a bulk monolith hydrogel is formed by diluting the solution either with water or
15 119 phosphate buffer saline (PBS) forming spherical nanoMIPs[27]. Others[28] have also
16 120 developed a method that works in a similar way oil/water Pickering emulsions, using
17 121 temperature responsive N-isopropylacrylamide (NIPAM) monomer and programmed ramped
18 122 temperature changes and careful timing with the addition of the initiators to form these
19 123 molecularly imprinted microgels (MIGs) or nanoMIPs with an imprinting factor (MIP versus
20 124 NIP of 2:1). Herein we demonstrate that nanoMIPs can be produced at room temperature in
21 125 aqueous solution. There can be a tendency to produce polydisperse particles sizes with
22 126 varying affinities for target template. We address this here by using a series of nano-filters to
23 127 size separate the nanoMIPs. We demonstrate a nanoMIP size dependency leading to higher
24 128 affinities.

25
26
27
28
29
30
31
32
33
34
35 129 Despite offering superior affinities compared to the bulk MIP approach [18], both bulk MIP
36 130 and nanoMIP methods face challenges in seamless integration with sensors. The layering of
37 131 nanoMIPs onto sensor surfaces poses a significant challenge, necessitating additional surface
38 132 chemical modifications. For instance, this can involve the use of 11-mercaptoundecanoic acid
39 133 followed by a coupling procedure employing 1-ethyl-3-(3-dimethylaminopropyl)
40 134 carbodiimide (EDC)/N-hydroxysuccinimide (NHS) to attach the MIPs to the sensor chip
41 135 surface. The EDC/NHS methodology has been reported in sensor systems such as quartz
42 136 crystal microbalance (QCM), surface plasmon resonance (SPR) chips, electrochemical
43 137 electrodes, and screen-printed electrodes[29, 30]. We have addressed this here by physically
44 138 entrapping the nanoMIP on an electrode in an electropolymerized thin-film matrix. Whereas
45 139 both methods are appropriate for the attachment of nanoMIP to a gold electrode surface,
46 140 there are several advantages for the physical trapping method we used. First, it is an
47 141 electrochemical method allowing fine control of layer-by-layer deposition of an
48 142 electrochemically grown layer (E-layer) in order to physically entrap the nanoMIP
49 143 particles[15]. Given the chemical nature of the E-layer used being like the nanoMIP, there is
50 144 natural compatibility between the two materials ensuring facile integration and minimising
51 145 rejection. With EDC/NHS chemical coupling, subsequent surface blocking steps are required
52 146 to passivate the unused surface requiring ethanolamine and/or serum albumin as a blocking
53 147 agent to minimise non-specific binding[31, 32]. However, with physical entrapping the E-layer

1
2
3 148 formed around the nanoMIP particles offers a dual purpose of locking the nanoMIP down to
4 149 the surface region and also passivating unused surface.

6
7 150 Efforts to scale up the production of functional nanoMIPs for commercial applications, such
8 151 as diagnostics, imaging and biological extractions is ongoing. While some progress has been
9 152 made, particularly with nanoMIPs using a microgel synthesis processe in solution, existing
10 153 methods suffer from low milligram yields and lengthy (days) production times[28].

12
13 154 To address this, we have developed and improved these existing approaches to deliver a
14 155 method with improved yields of high affinity protein-selective nanoMIPs that can be easily
15 156 integrated with electrochemical sensors resulting in sub-picomolar determinations of target.
16 157 Antibody-like affinity is confirmed by electrochemical determination of K_D . A comparison is
17 158 made with K_D values determined using surface plasmon resonance.

19
20 159 Our advances represent a significant step toward addressing the scalability challenges
21 160 associated with nanoMIP production, paving the way for broader adoption and application in
22 161 various industries.

24 162 **2.Experimental**

25 163 **2.1 Materials**

26
27 164 N-hydroxymethylacrylamide (NHMA, 48% w/v), N,N'-methylenebisacrylamide (MBAm),
28 165 phosphate buffered saline tablets (PBS, 10 mM, pH 7.4 ± 0.2), methylhydroquinone (MHQ),
29 166 potassium ferricyanide ($K_3Fe(CN)_6$), potassium chloride (KCl), sodium nitrate ($NaNO_3$),
30 167 potassium peroxydisulfate (KPS), sodium dodecyl sulphate (SDS), acetic acid (AcOH),
31 168 ammonium persulphate, Tetramethylethylenediamine(TEMED), haemoglobin from bovine
32 169 species, and buffers (PBS, HEPES and Tris) were all purchased from Merck Ltd. Buffers were
33 170 prepared in E-pure water (resistivity $18.2 \pm 0.2 M\Omega.cm$). DropSens disposable screen-printed
34 171 electrodes (SPEs) (Au-AT & Au-BT) comprising a gold working electrode (4 mm diameter), a
35 172 platinum counter electrode and silver reference electrode were purchased from Metrohm
36 173 (Runcorn, Cheshire).

37 174 **2.2 Nanogel (NanoMIP and NanoNIP) Synthesis**

38
39 175 Nanogels were synthesized via radical polymerization using N-hydroxyethylmethacrylamide
40 176 (NHMA) as the monomer, bovine hemoglobin (BHb) or bovine serum albumin (BSA) as the
41 177 template protein, and N,N'-methylenebisacrylamide (MBAm) as the crosslinker. Specifically,
42 178 1.080 g of NHMA, 0.24 g of BHb (or BSA), and 0.12 g of MBAm were dissolved in 20 mL of
43 179 phosphate-buffered saline (PBS, pH 7.4) containing 0.0037 g sodium dodecyl sulfate (SDS).
44 180 The solution was stirred continuously under a nitrogen atmosphere. Radical initiation was
45 181 initiated by adding 400 μL of 20% (v/v) tetramethylethylenediamine (TEMED) and 10% (w/v)
46 182 ammonium persulfate (APS). The reaction vessel was sealed with parafilm, leaving a 1 cm
47 183 headspace to prevent pressure buildup, and the mixture was stirred vigorously for 1 min.
48 184 The stirring rate was then reduced to 250 rpm, and aliquots (500 μL) of the reaction mixture
49 185 were withdrawn at defined time intervals (5, 7, 10, 15, and 20 minutes). Each aliquot was
50 186 immediately quenched with an equal volume (500 μL) of 10 mM methoxyhydroquinone

187 (MHQ). Polymerization was monitored until the reaction mixture turned cloudy, indicating
188 completion (approximately 20 min).

189 The polymerization products were analyzed using a BioDrop μ LITE UV-visible spectrometer to
190 confirm polymer formation. Upon reaction completion, the remaining mixture was quenched
191 with an excess of 20 mL of 10 mM MHQ.

192 **2.3 Spectrophotometric Characterisation of NanoMIP**

193 NanoMIP synthesis was optimized for a 15-minute reaction time. Aliquots (1 mL) of the
194 reaction mixture were quenched, centrifuged at 15,000 rpm, and the supernatant
195 discarded. The pelleted NanoMIPs were treated with 5 mL of a denaturing solution
196 comprising 10% (w/v) SDS and 10% (v/v) acetic acid to elute the template protein. Following
197 centrifugation (15,000 rpm), the supernatant was collected for spectrophotometric analysis
198 at 395 nm, a wavelength chosen to account for the denatured protein's absorbance shift
199 [18]. The washing/elution procedure was repeated five times, and subsequent washes with
200 ultrapure water (≥ 5 cycles) were conducted to remove residual SDS. The efficacy of SDS
201 removal was confirmed by KCl precipitation tests [33]. Finally, the purified NanoMIPs were
202 resuspended in 1 mL PBS.

203 An alternative protein elution method using sonication was also investigated. NanoMIPs
204 were washed with ultrapure water and subjected to sonication at 30 °C for 15 min, followed
205 by centrifugation and supernatant removal. This procedure was repeated five times, and the
206 amount of eluted protein was analyzed spectrophotometrically at 406 nm, a wavelength
207 indicative of intact, non-denatured protein.

208 Following protein elution, NanoMIPs (1 mL) were reloaded with BHb (1 mg/mL) for 30 min
209 to assess template protein rebinding. The percentage of protein rebound (%Rebind) was
210 calculated spectrophotometrically (at 406 nm for BHb) using the formula:
211 %Rebind=100 x (O-R/O), where O represents the initial protein concentration, and R
212 represents the residual protein concentration post-rebinding.

213 **2.4 Size selection of nanoMIPs using Extrusion Filtration.**

214 1 mL of the protein-eluted and sonicated nanoMIP mixture was taken through a mini extruder
215 (Avanti Polar Lipids, Inc.) with decreasing filter sizes of 800 to 100 nm (2-5 min process for
216 each filter size). Starting with the largest pore size filter (800 nm), the residue collected on
217 the membrane was suspended into epure water (1mL) using sonication. The filtrate was then
218 sequentially passed through smaller filters repeating the same process, using 400 nm, 200 nm
219 and then 100 nm pore size membranes. The residue on the membrane thus collected at each
220 stage were expected to give batches of particles ranging in size > 800 nm (on 800 nm filter);
221 400-800 nm (on 400 nm filter); 200-400 nm (on 200 nm filter); 100-200 nm (on 100 nm filter);
222 and < 100 nm (the final filtrate). Each batch was lyophilised for subsequent dynamic light
223 scattering size measurement and electrochemical characterisation. Figure 1 gives a summary
224 of the process followed to obtain nanoMIPs at various filter sizes.

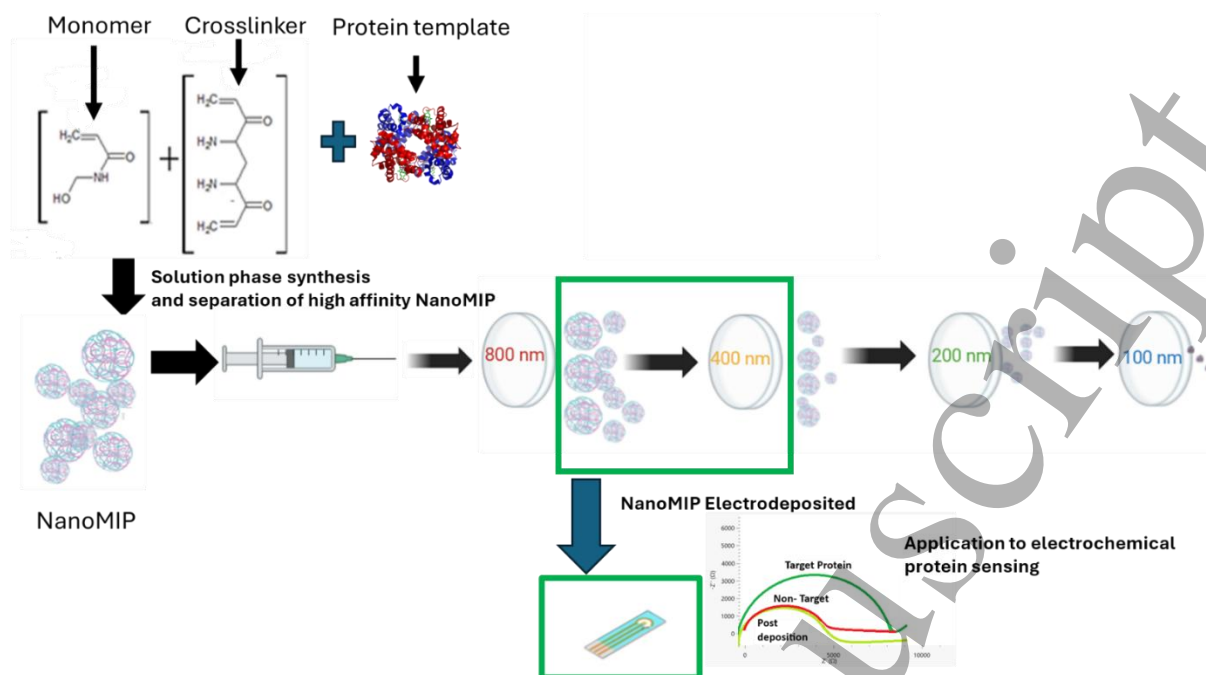


Figure 1: Schematic representation showing nanoMIP synthesis and subsequent isolation of different size nanoMIPs where the initial polydisperse mixture is passed through progressively smaller filters from 800nm-100nm allowing for size selection of the produced nanoMIPs. Subsequent biosensor application of optimised nanoMIP illustrated.

2.5 NanoMIP Lyophilisation and Yield Determination

The nanoMIP solution flash frozen in liquid nitrogen followed by lyophilisation using a CHRIST Alpha 2-4 LDplus freeze-dryer. The Eppendorf tube, with opening covered with Parafilm® and pierced was then placed in the freeze dryer at -90 °C and at low pressure (0.011 mbar) until a fine fluffy off-white powder was produced (16hr). The mass of the lyophilised powder was then determined.

2.6 Dynamic Light Scattering characterization of NanoMIPs

The hydrodynamic size of NanoMIPs was determined using a Zetasizer Nano ZS. Lyophilized NanoMIPs were resuspended in PBS, and measurements were performed in triplicate using a disposable cuvette (refractive index: 1.32). The samples were equilibrated for 60 s prior to measurement.

2.7 Electrochemical Deposition and Analysis of NanoMIP

Electrochemical experiments were conducted using a Metrohm Autolab PGSTAT204 potentiostat with NOVA2.1.4 software. NanoMIP-modified electropolymerized layers (E-layers) were fabricated on BT-Au screen-printed electrodes (SPEs) by cyclic voltammetry (CV), following a previously reported procedure [15]. A solution (50 μ L) containing 0.1 mg NanoMIP, 1.33 M NHMA, 41.5 mM MBAm, 0.29 M NaNO₃, and 48.15 mM KPS in PBS was deposited on the SPE surface (Fig. 1). Potential was cycled between -0.2 V and -1.4 V for 7

249 cycles at 50 mV/s (10 min, RT, 22 ± 2 °C). Control E-layers (without NanoMIPs) were also
250 prepared.

251 The NanoMIP-modified electrodes were exposed to varying concentrations of BHb (100 fM–
252 100 μ M) for 5 min, followed by rinsing and analysis using electrochemical impedance
253 spectroscopy (EIS) to assess protein binding (Fig. 1). Selectivity was investigated using EIS in
254 5 mM potassium ferricyanide solution containing 0.5 M KCl, with data analyzed using a
255 Randles equivalent circuit model.

256 **2.8 AFM Images**

257 AFM imaging of bare and NanoMIP-coated electrode surfaces was performed in liquid (PBS)
258 using a Bruker Dimension Icon® with NanoScope 6 controller. PeakForce Tapping™ mode was
259 employed with silicon nitride cantilevers (SCANASYST-FLUID, nominal spring constant 0.7
260 N/m). The coated electrodes were prepared as described in **Section 2.7** and imaged with and
261 without NanoMIP entrapment.

262 **2.9 Surface Plasmon Resonance Binding Affinity Studies**

263 Using a Reichert 2 SPR system (Reichert Technologies, Buffalo, USA) surface plasmon
264 resonance (SPR), experiments were performed using an adapted methodology, to provide
265 accurate binding affinities of the imprinted materials. A carboxymethyl dextran hydrogel
266 coated Au chips were installed as per the manufacturer's instructions. A running PBST (PBS
267 pH 7.4 and 0.01 % Tween 20) was flowed over the sensor surface at 10 μ L min⁻¹ until the
268 baseline was stable, with this flow rate of 10 μ L being maintained throughout the
269 immobilisation process. For the immobilisation of the nanoMIP, a fresh solution of EDC (40
270 mg) and NHS (10 mg) dissolved in 1 mL water was injected onto the sensor chip surface for 6
271 minutes, this enables the activation of carboxyl groups contained within the carboxymethyl
272 dextran layer. Next the nanoMIP (300 μ g) dissolved in 1 mL of the running buffer (PBST) and
273 10 mM sodium acetate (0.82 mg mL⁻¹), was injected only to the left channel of the activated
274 surface for 1 minute. To deactivate the surface a quenching solution (1 M ethanolamine, pH
275 8.5) was then injected for 8 min enabling the deactivation of the carboxyl groups. This provide
276 a sensor surface with nanoMIP immobilised onto the left channel as the working channel,
277 while the right channel is used as a reference control.

278 Binding kinetic analysis performed using an existing
279 methodology and initiated by injection of the running buffer PBST (blank) onto the nanoMIP
280 immobilised sensor surface with a 2 min association, followed by a 5 min dissociation. The
281 binding kinetics of the individual nanoMIPs towards the analyte (BHb) was determined from
282 the association of analyte between 4-64 nM of BHb. After dissociation a regeneration buffer
283 (10 mM Glycine-HCl, pH 2) was used to remove the analyte from the nanoMIP, thus renewing
284 the sensor surface.

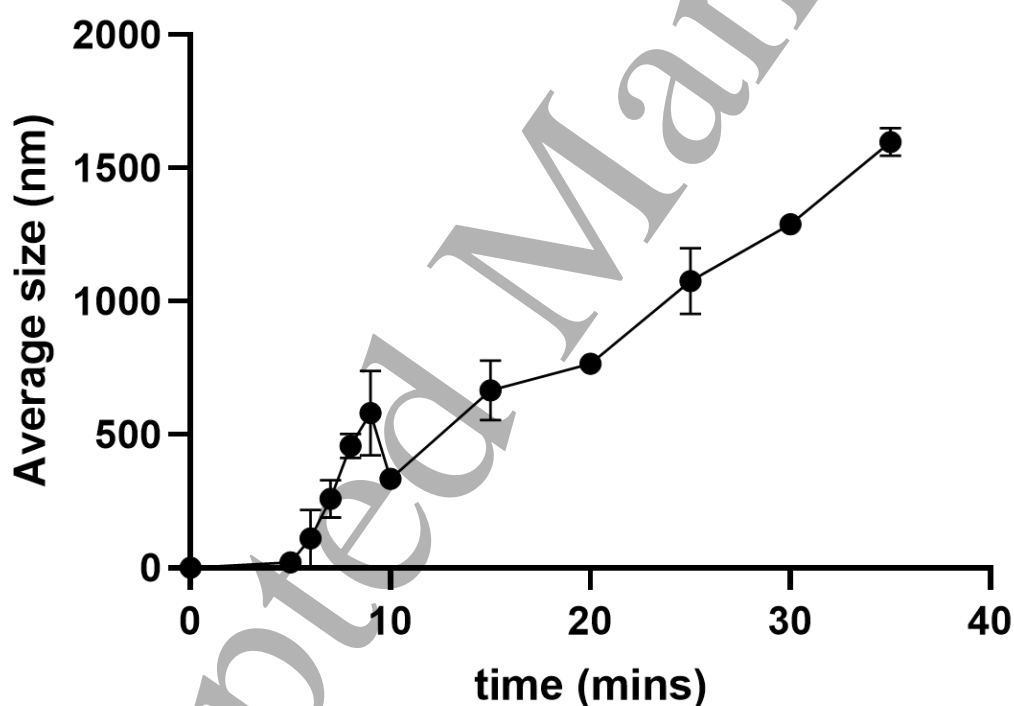
285 Signals from the working channel (left) were subtracted with those of the respective
286 reference channel (right), to reveal the specific binding of the nanoMIP. The SPR responses
287 were fitted using a 1:1 Langmuir bio-interaction (BI) model using TraceDrawer Software.
288 Association rate constant (k_a), dissociation rate constant (k_d), and maximum binding (B_{max})

289 were fitted globally, whereas the BI signal was fitted locally. The equilibrium dissociation
290 constant (K_D) was calculated from k_d/k_a .

291 3. Results and Discussions

292 3.1 NanoMIP Production and Optimisation

293 Previously published microgel synthesis methods [34, 35] were adopted and modified for
294 the preparation of nanoMIPs. We report for the first time the use of extrusion methods to
295 to size-select and purify nanoMIPs. Parameters such as synthesis time and use of a
296 quenching agent were found to be important in delivering nanoparticles with reduced
297 variability in average size according to DLS measurements. Aliquots were taken and reaction
298 terminated using methyl hydroquinone each time point displayed. Fig 2 shows the averaged
299 size for particles at each time point. Detectable particles were only produced after an initial
300 lag of 5 minutes. It should be noted that even though the averaged hydrodynamic particle
301 diameter was increasing with increased reaction time, it was clear from DLS measurements
302 that a range of particle sizes were being produced throughout the process. Figures S1-S5
303 compare DLS spectra at time points 5, 7, 10, 15 and 20 min.



304
305 Fig 2. Increase in average gel hydrodynamic particle diameter with increasing synthesis time prior
306 to MHQ quenching of reaction. Figs S1 to S5 show a selection of representative DLS spectra at time
307 points 5, 7, 10, 15 and 20 min synthesis times respectively. The synthesis was conducted in triplicate,
308 yielding three DLS spectra per synthesis time. Each data point in Fig 2 is therefore the average
309 hydrodynamic diameter from three sets of DLS spectra for each synthesis time (Data represents
310 mean \pm S.E.M., $n = 3$).

311 We attribute the presence of large particles at short reaction times to second order
 312 processes subsequent to chemical reaction where particles are tending to aggregate. The
 313 extent of aggregation increases with nanoMIP particle synthesis time. In order to minimise
 314 the concentration of large agglomerates, we selected the reaction termination time of 15
 315 minutes.

316 Prior to any separation of particles into size batches, we looked to optimise protein elution
 317 and rebinding conditions of the parent batch. We demonstrate here a move away from
 318 using conventional harsh elution conditions with SDS/AcOH [18] to the application of
 319 sonication to release template protein from the nanoMIP. Sonication at 30 °C demonstrated
 320 an almost identical protein elution profile to using SDS/AcOH (Fig 3a). Subsequent target
 321 rebinding studies demonstrated that sonicated nanoMIP was only 10% less effective at
 322 rebinding BHb than SDS/AcOH washed nanoMIP (Fig 3b). Given the reduced need for
 323 reagents without significantly affecting rebinding properties, we selected the use of
 324 sonication and mild heating to elute the non-covalently bound target protein.

325

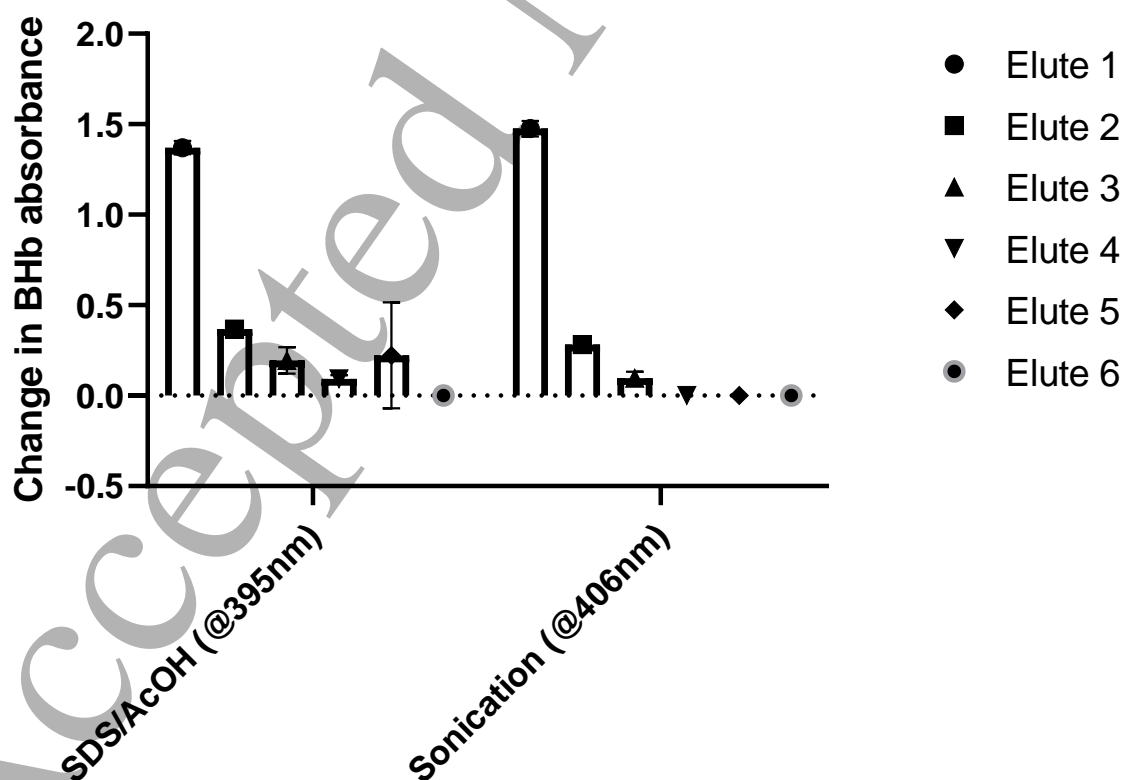
326

327

328

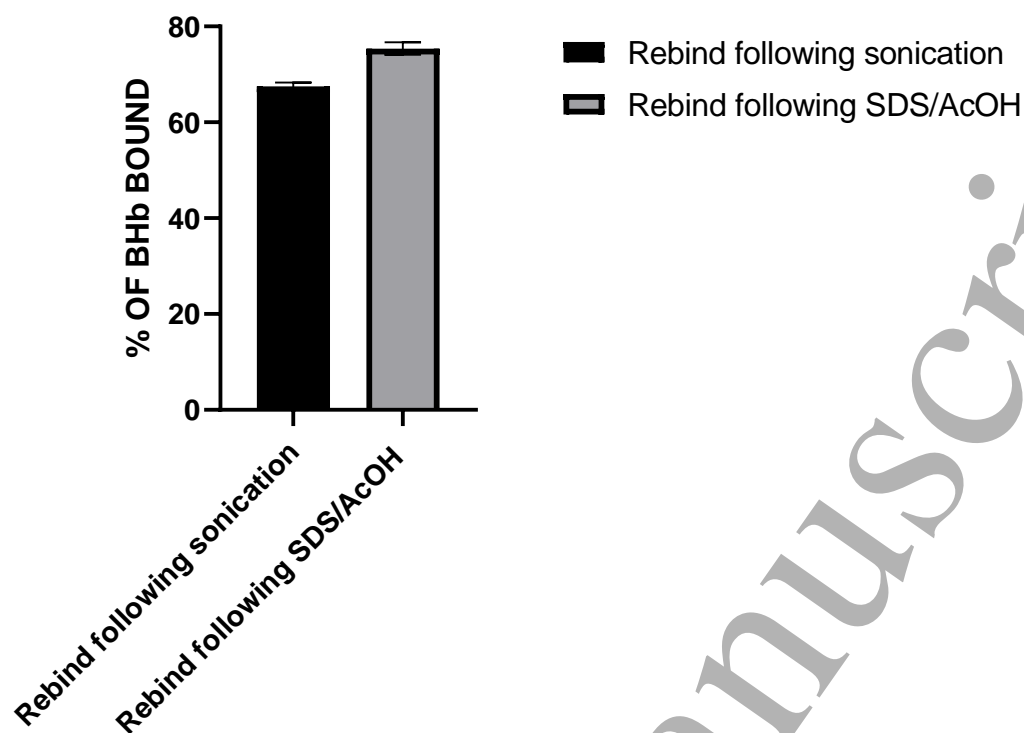
329

330 Fig 3a



331

332 Fig 3b



333
 334 **Fig 3. Comparison of the effect of SDS/AcOH and sonication with mild heating on (a) protein**
 335 **elution and (b) subsequent protein rebinding in PBS. % rebind was determined**
 336 **spectrophotometrically (at 406 nm for BHB) by measuring amount of protein remaining in**
 337 **solution after rebind (R) and comparing against original protein reload (O) using the**
 338 **equation $100 \times (O-R/O)$. Data represents mean \pm S.E.M., n = 3.**

339
 340 To further optimise rebinding conditions, we investigated the effect of buffer solution used
 341 on protein rebinding to nanoMIP. We investigated PBS, HEPES buffer and Tris buffer all at
 342 pH 7.4. Deionised water only was also tested. Fig 4 shows HEPES buffer was not an effective
 343 support medium for rebinding of protein to pNHMA based nanoMIPs. PBS showed
 344 nanoMIPs to be 80% effective at protein rebinding whereas Tris buffer demonstrated that
 345 the nanoMIPs were 10% less effective than PBS and approximately 10% more effective than
 346 water only. The conformational stability of proteins has been known to increase if anionic
 347 buffers are used above the pI of the protein (and conversely, if cationic buffers are used
 348 below the pI)[36]. At its pI, a protein is electrically net neutral containing a balance in
 349 charge between carboxyl and amide groups existing as $-\text{COO}^-$ and $-\text{NH}_3^+$ respectively.
 350 Above their pI however, proteins become negatively charged and the groups exist as $-\text{COO}^-$
 351 and $-\text{NH}_2$ respectively. BHB has a pI of 7.1 and therefore at pH 7.4 has an overall slight net
 352 negative charge. This overall negative net charge induces more favourable and
 353 complementary hydrogen bonding interactions between protein and the nanoMIP polymer
 354 At pH 7.4, the partially protonated phosphate buffer or the Tris buffer (pKa of 8.1) with its

three un-dissociated hydroxyl groups appear suitable for improving MIP selectivity by providing optimum specific binding and reducing non-specific binding interactions. It is plausible that the PBS and Tris buffer systems are aiding in stabilising the native protein structure within the nanoMIP binding site. However, the poor rebinding of BHb with HEPES is remarkable. We propose that at the binding site of the nanoMIP, there is a net anionic repulsion between the protein and the prominent sulphonate group of HEPES buffer molecules resulting in poor capture of protein by nanoMIP. Due to optimum rebinding of protein in PBS, we used pNHMA nanoMIPs in PBS going forward.

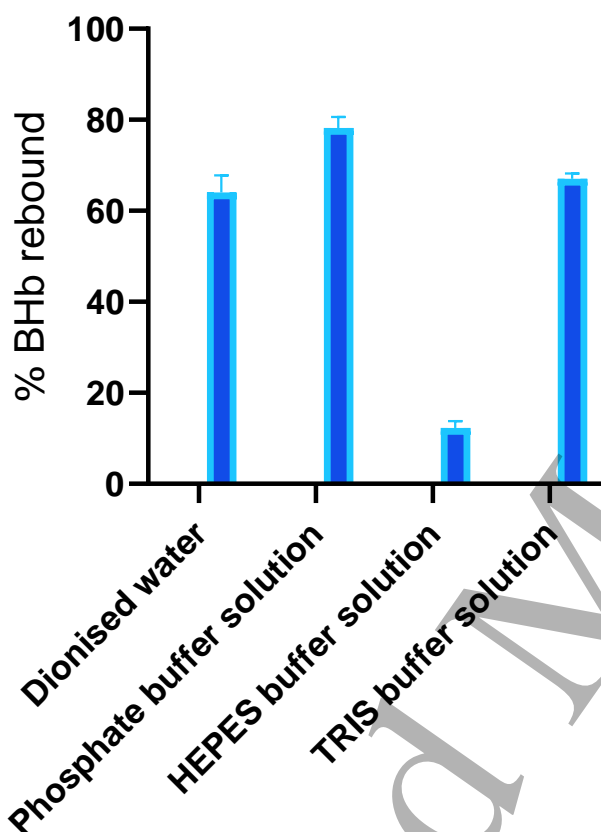


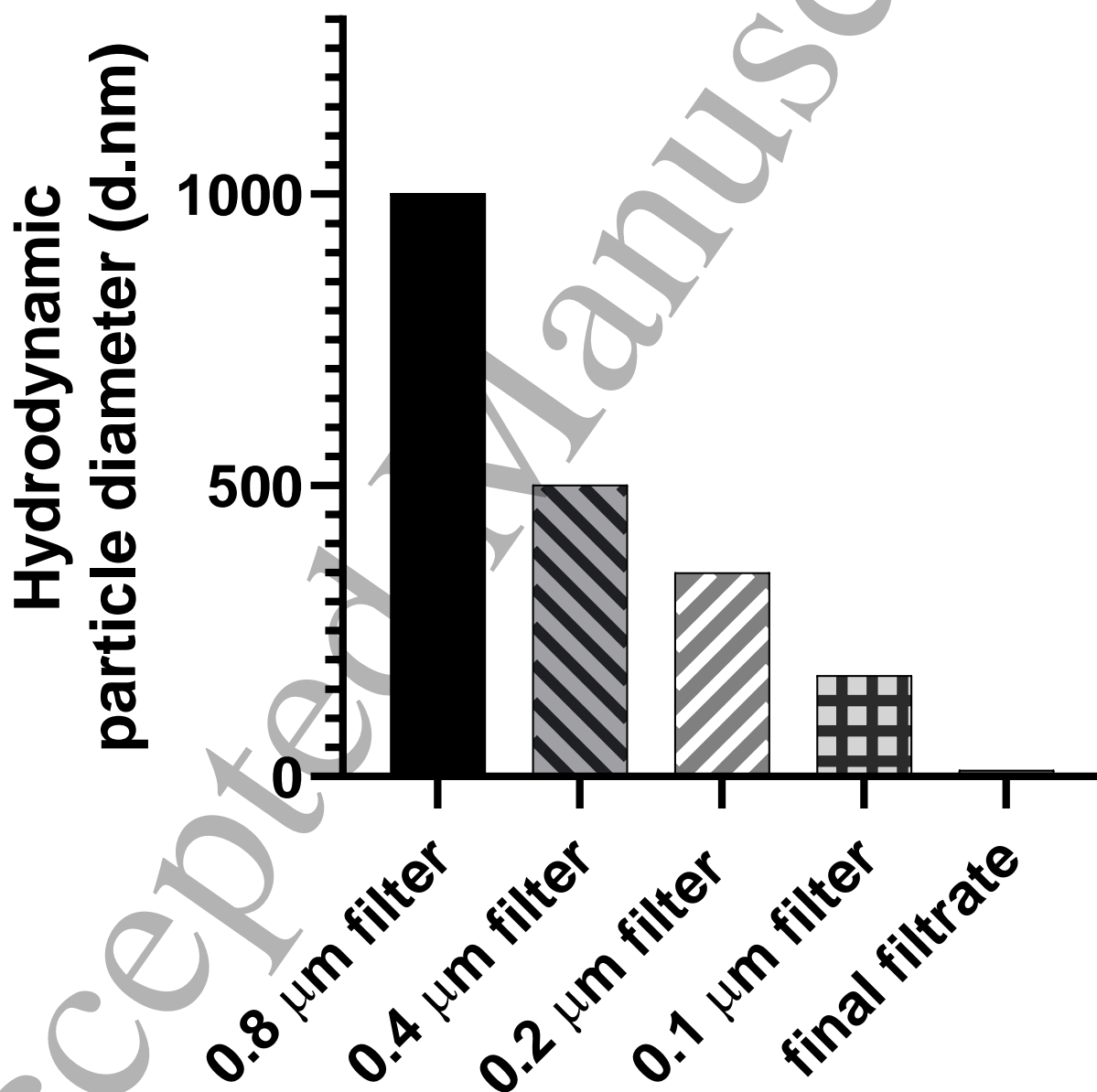
Fig. 4. Effect of buffer composition on % target protein rebinding on BHb nanoMIPs. % rebind was determined spectrophotometrically (at 406 nm for BHb) by measuring amount of protein remaining in solution after rebind (R) and comparing against original protein reload (O) using the equation $100 \times (O-R/O)$. Data represents mean \pm S.E.M., n = 3.

3.2 NanoMIP Particle Size Selection and Dynamic Light Scattering Studies

We then investigated the effect extrusion filtering (taking 2-5 min) through microporous polycarbonate membranes (800 nm to 100 nm) as a method to successively narrow the size range of nanoMIP particles in the parent sample (Fig. 1). The residue on the membrane thus collected at each stage were expected to give batches of particles ranging in size greater

1
2
3 375 than 800 nm (on 800 nm filter); 400-800 nm (on 400 nm filter), 200-400 nm (on 200 nm
4 376 filter) and 100-200 nm (on 100 nm filter). The final filter used was 100 nm in pore size
5 377 ensuring the filtrate contained only particles of less than 100 nm. Each batch and the final
6 378 filtrate were lyophilised for subsequent dynamic light scattering size measurement and
7 379 electrochemical characterisation. A fraction (0.1 mg) of each lyophilised sample was
8 380 resuspended in PBS for DLS analysis. Fig. 5 shows the effect of using various pore sized
9 381 polycarbonate filters to isolate nanoMIPs. The filtration technique was effective in
10 382 minimising aggregation of particles.

383



384

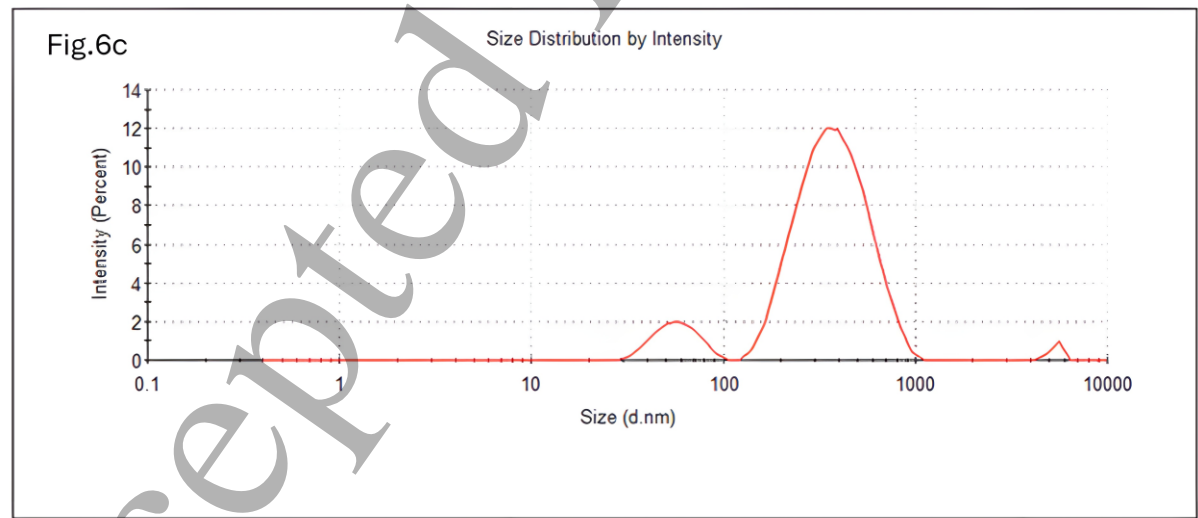
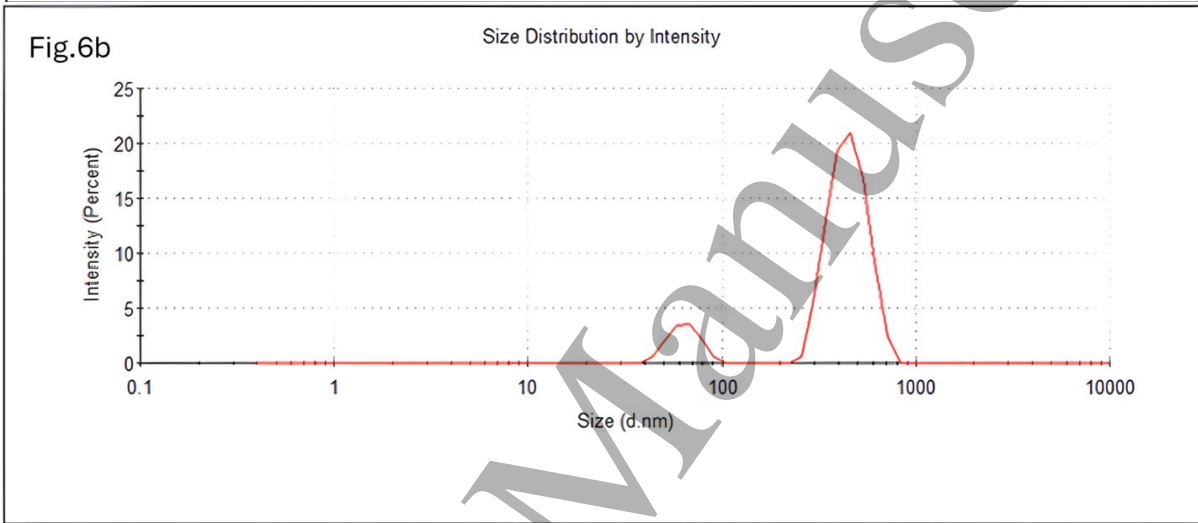
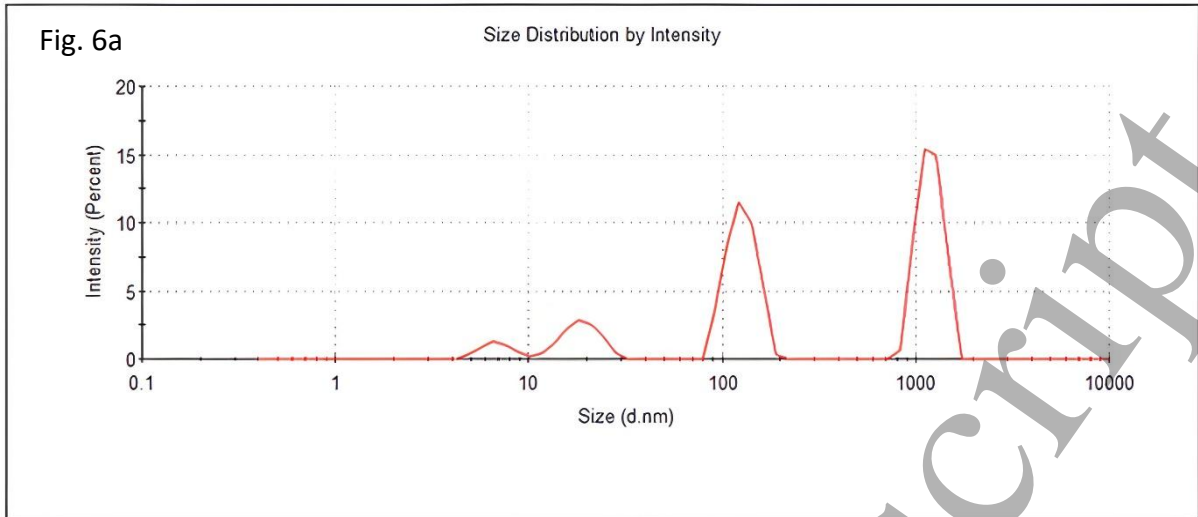
385 Fig. 5. DLS particle sizing of fractions collected on sequential filters with decreasing pore
386 size (800 nm to 100 nm) and final filtrate emanating from the last filter (100 nm). Fractions

1
2
3 387 **collected on each subsequent filter were sonicated and resuspended in buffer prior to DLS**
4 **388 sizing. The filtrate from the filter was then passed through the next filter down and the**
5 **389 collection/DLS process repeated.**
6
7

8 390 Whilst the plot in Fig. 5 gives a snapshot average of the hydrodynamic particle diameter in
9 391 any fraction collected, the real situation is best captured from the raw DLS data (Figure 6 (a-
10 392 e) which show a range of hydrodynamic particle diameters for each collected residue
11 393 (unfiltered material) and the final filtrate. Fig 6a analyses the unfiltered material following
12 394 filtration of nanoMIP crude sample through a 800 nm filter. Fig 6a shows a multimodal
13 395 distribution of nanoMIP hydrodynamic particle diameters collected by the 800 nm filter
14 396 suggesting that the larger particles (> 800 nm) were blocking the filter and impeding the
15 397 permeation of some (but not all) of the smaller particles. Fig. 6b analyses the unfiltered
16 398 material following filtration of the 800 nm filtrate through a 400 nm filter. We observe a
17 399 bimodal distribution of nanoMIP particles in the range 30-100 nm and a very broad peak in
18 400 the range 110 nm to 800 nm. Fig 6c analyses the unfiltered material following filtration of
19 401 the 400 nm filtrate through a 200 nm filter. Again, we observe a similar bimodal distribution
20 402 of nanoMIP particles sizes. Fig 6d analyses the unfiltered material following filtration of the
21 403 200 nm filtrate through a 100 nm filter. Here we observe a single peak between 100-200 nm
22 404 centred around 150 nm indicative of a homogeneous nanoMIP particle size. And finally, Fig
23 405 6e analyses the final filtrate emanating from the 100 nm filter. Interestingly, we observe a
24 406 biomodal distribution of very small nanoMIP particles centred at 1.0 and 20 nm. However,
25 407 the intensity of the peak at 1.0 nm is small representing an insignificant yield of particles
26 408 and can be discarded.
27
28
29
30
31
32

33 409

34 410
35
36
37
38
39
40
41
42
43
44
45
46
47
48
49
50
51
52
53
54
55
56
57
58
59
60



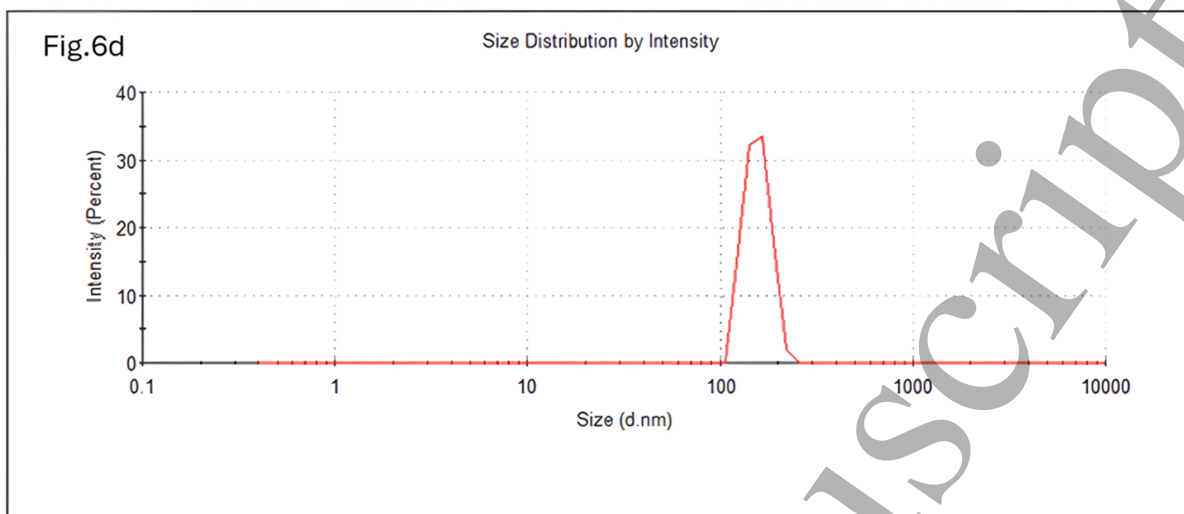
411

412

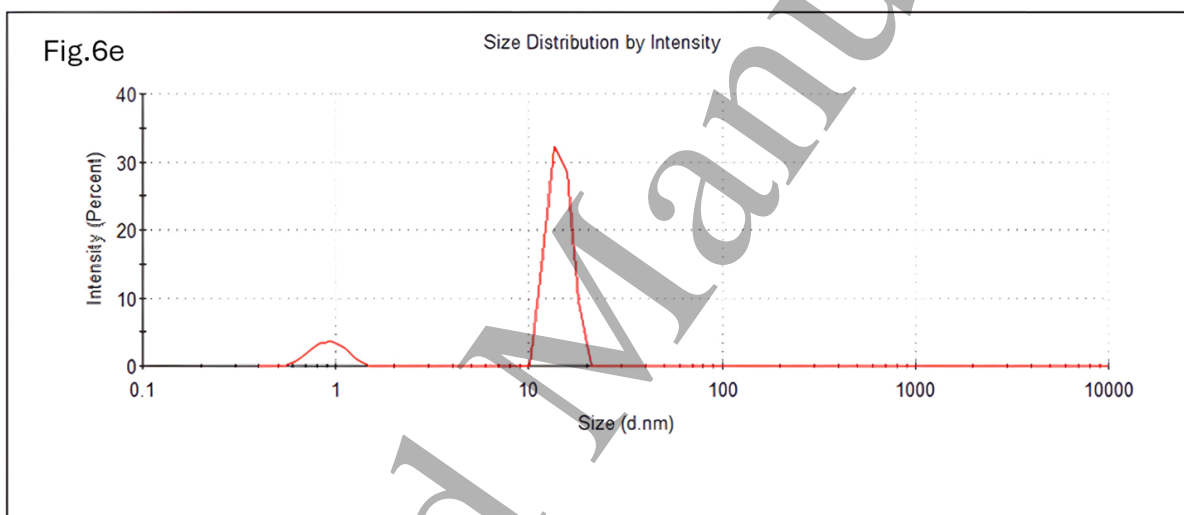
413

414

415

416
417

418



419

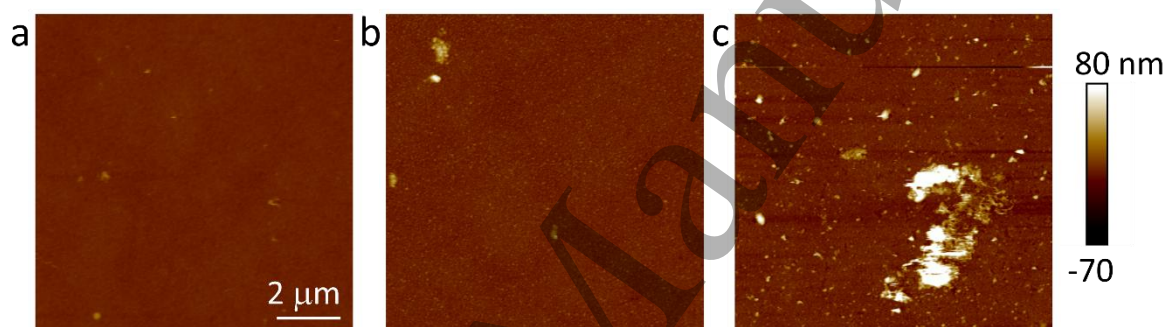
420 **Fig. 6.** DLS spectra of fractions collected on sequential filters with decreasing pore sizes
421 showing nanoMIP hydrodynamic particle diameter distribution for (a) 800 nm, (b) 400 nm
422 (c) 200 nm and (d) 100 nm; and (e) final filtrate emanating from the last filter (100 nm).

423

424 3.3 Electrochemical Binding Affinity Studies

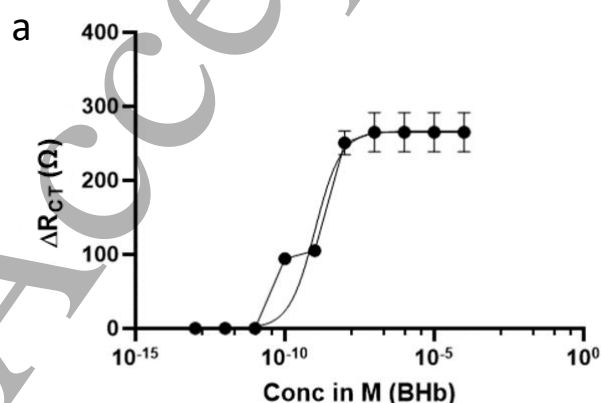
425 The next stage was to test the rebinding affinity of each batch. Whereas the unfiltered
426 parent batch was easy to pellet for UV/Vis characterisation of rebinding, the filtered batches
427 (< 800 nm) did not pellet. In order to test the rebinding efficiency of these particles, we used
428 a modified form of our previously published electrochemical method [15]. In our previous
429 method, we produced electrochemically grown thin film MIPs on disposable screen-printed
430 electrodes selective to target proteins. We used acrylamide-based monomers and the
431 resulting thin film itself was the MIP. Rebinding of protein was evaluated using
432 electrochemical impedance spectroscopy in the presence of ferrocyanide as redox marker.

433 The increase in charge transfer resistance (R_{CT}) was directly proportional to increased target
 434 protein binding. Here, we adapted this method by using the electrochemically produced
 435 thin film method to physically entrap nanoMIP at the electrode surface. One hundred
 436 microgrammes of each lyophilised batch was resuspended in 1000 μ L of PBS containing
 437 NHMA monomer, bisacrylamide crosslinker and potassium persulphate (KPS) initiator. Cyclic
 438 voltammetry was used with a reduction cycle between -0.2 to -1.2 V to electrochemically
 439 induce KPS to produce sulphate radicals ($SO_4^{\cdot-}$) which in turn initiated chemical
 440 polymerisation of NHMA/bis at the electrode surface. Seven cycles were used to produce a
 441 thin film that physically entrapped nanoMIPs *in-situ* (See Fig S6). Fig 7a shows AFM of a bare
 442 gold electrode surface. Whereas the E-layered electrode is relatively smooth with few
 443 discernible features in the absence of nanoMIP (Fig 7b), in the presence of nanoMIP
 444 captured on a 200 nm membrane (Fig. 7c), many particles are observable typically ranging in
 445 size from 100 to 200 nm, with some larger particles measured with heights greater than 900
 446 nm. We believe that the large particles are the result of some aggregation or coalescence of
 447 smaller nanoparticles (Fig S7).

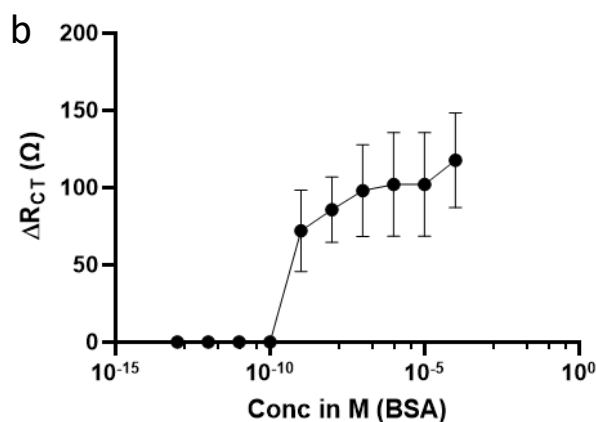


448
 449 **Fig. 7. AFM micrographs of gold electrode (a), gold electrode E-layer surface in the**
 450 **absence of entrapped nanoMIP (b) and gold electrode E-layer surface in the presence of**
 451 **entrapped nanoMIP (c).**

452 The nanoMIP entrapped E-layer was tested for target and non-target protein rebinding. We
 453 observed a concentration dependent change in R_{CT} from 1pM to 1 nM target protein
 454 addition (Fig. 8a). In the presence of non-target protein over the same concentration range
 455 there was a much-reduced signal (Fig 8b). For example, at 1 nM protein level, the selectivity
 456 factor (response to target divided by response to non-target) was acceptable at 3:1.



464
465



466

Fig 8. Concentration dependent change in R_{CT} for target, BHb (a) and non-target, BSA (b) binding to BHb NanoMIP. Data represents mean \pm S.E.M., $n = 3$. Figure S8 shows the cumulative Nyquist plot data from which the R_{CT} was calculated. In each Nyquist plot there is a semi-circle arc, the diameter of which is indicative of the charge transfer resistance (R_{CT}) value. R_{CT} gives an indication of the ease with which the electrolyte and redox marker can be transported to the electrode surface.

473

The sensor LOQ was determined to be 1 pM, with an LOD of 100 fM. The signal plateaued beyond 10 nM and indicated that saturation in selective surface binding had occurred. Further, we investigated using the Hill-Langmuir method to determine K_D for nanoMIP. Assuming the latter was the maximum protein binding capacity of the E-MIP thin film (B_{max}), we can use the Hill-Langmuir method to determine the equilibrium dissociation constant K_D for the E-MIP. We assumed the Hill coefficient is equal to 1, which is indicative of ligand (MIP) binding with no cooperativity to one site. The K_D was then determined from the plot to be the protein concentration associated with 50% of binding sites being occupied ($B_{max}/2$). The calculated K_D was determined to be 1.03 ± 0.4 nM.

Subsequently, each of the larger filtered batch sizes of nanoMIP were investigated electrochemically for yield, rebinding and selectivity using E-layer entrapment. Table 1 summarises the results. Some of the material collected on the 800 nm filter was prone to excessive clumping and sedimented immediately even after sonication. Whereas the yield was high (4.6 mg/mL) the material characterised for this fraction was very much representative of a mixed phase of particles ranging in size 100 nm to >800 nm giving low selectivity overall when tested on the electrochemical sensor. Selectivity was optimum when using the nanoMIP material collected on the 400 nm (representing material captured that has a bimodal distribution of hydrodynamic particle diameters centred at 110 nm and 800 nm; see Fig 6b) and with acceptable yield (2mg/mL). Filter fractions using 200 nm and 100 nm filters also gave acceptable selectivities. The worst performer in terms of selectivity was the 800 nm filter residue and the worst performer for yield was the final filtrate

through the 100 nm filter. The latter is understandable given that particles at the lower filter size end are represented in the yields for the larger filter captures. We surmise that excessive filtration is not necessary and a two-stage filtration process using only the 800 nm followed by the 400 nm filters is required to deliver high selectivity materials.

Filter used to collect nanoMIP fraction	Yield (mg/mL)	Selectivity at 100 nM (target = BHb; non-target = BSA)	Predominant NanoMIP size (nm)
800 nm	4.6	2:1	> 800
400 nm	2	16:1	400-800
200 nm	2.6	8:1	200-400
100 nm	0.4	6:1	100-200
Final filtrate	0.2	6:1	1-100

Table 1. Effect of filter size on final yield and selectivity of nanoMIP. NanoMIP selectivity was determined by taking a ratio of electrochemical signal (ΔR_{CT}) for target (BHb) and non-target (BSA) protein binding.

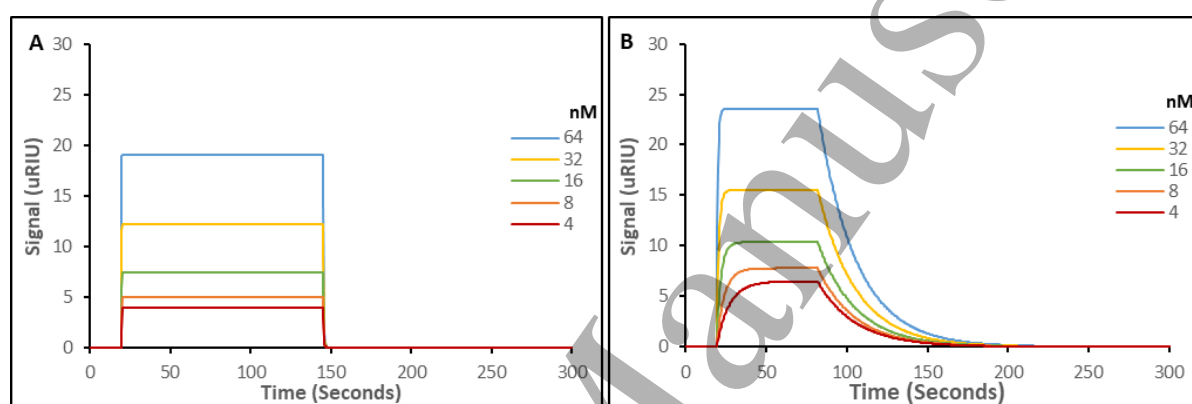
3.4 Surface Plasmon Resonance Binding Affinity Studies

For a comparison to be made between the above electrochemical method for determination of K_D and the generally accepted surface plasmon resonance method, the binding of the prepared nanoMIPs were investigated for their affinity towards the target protein (BHb) using SPR in a running buffer of PBS (pH 7.4) and Tween 20 (0.01%). The lyophilised nanoMIPs collected from the 200 nm filter were resuspended in 1 mL of the running buffer, with the addition of sodium acetate, before being deposited onto the SPR chip (coated in a carboxymethyl dextran layer). Deposition of the nanoMIPs onto the SPR chip surface is achieved through standardised carbodiimide coupling via an adapted Steglich esterification[37, 38] and occurs due to the high percentage of hydroxyl-functionality contained within the polymer composition of the nanoMIP. The pre-functionalisation of the gold SPR chips with a carboxymethyl dextran hydrogel layer enables for a good deposition profile, owing to the ease of activation of the dextran hydrogel by EDC/NHS. Ethanolamine is then used to deactivate any unwanted and unreacted carboxyl groups on the SPR chip surface, whilst also washing away any unbound nanoMIPs. Consistent with previous SPR-MIP binding studies, the initial deposition of nanoMIPs was added in excess to allow for full coverage on the chip, giving the maximum potential population of binding sites available per chip[39]. Thus, having a theoretical maximum receptor (binding population) allows for standard model for ligand/receptor interactions to be applied, enabling the application of a 1:1 kinetic binding model[40].

The SPR sensorgrams presented in Figure 9 shows the interactions of five different concentrations of the target molecule (BHb) with two batches of the nanoMIPs collected from the 200 nm filter, labelled Batch 1 and Batch 2 (Figure 9A and 9B, respectively), immobilised onto the surface of the SPR chip. From these curves and the application of a 1:1 model the

528 elucidation of the overall equilibrium dissociation constant (K_D) for the target interacting with
 529 their nanoMIPs and is summarised in Table 2. SPR binding affinity studies could only be
 530 performed on the 200 nm filtered batch simply because the SPR penetration depth will not
 531 be able to reach the surface of the 400 and 800 nm filtered batches of nanoMIPs. The
 532 penetration depth of traditional SPR chips is approximately 216 nm[41]. There have been
 533 significant advances in SPR chip production that have allowed the penetration depths to
 534 increase[42]. However, increasing sensitivity to allow for a greater probing depth has yet to
 535 reach the limit of greater than 400 nm. To explore specificity of the nanoMIP, the cross-
 536 reactivity and non-specific binding was also investigated through the loading of a non-target
 537 protein (BSA) onto the nanoMIP coated chip. The K_D values for the binding of the non-target
 538 (BSA), is also represented in Table 2, with SPR sensorgrams shown in Figure S9.

539



540

541

542 **Fig. 9. Representative SPR curves showing the rebinding of the target protein (BHb) to the**
 543 **immobilised nanoMIPs. Five concentrations of analyte in PBST. (A) BHb binding to BHb-**
 544 **imprinted nanoMIP (Batch 1); (B) BHb binding for BHb-imprinted nanoMIP (Batch 2).**

545

546

547

548

549

550

NanoMIP	K_D value (M)	
	BHb	BSA
Batch 1	$2.75 \times 10^{-9} (\pm 0.85 \times 10^{-9})$	$6.21 \times 10^{-7} (\pm 0.23 \times 10^{-6})$
Batch 2	$2.20 \times 10^{-9} (\pm 0.20 \times 10^{-9})$	$2.64 \times 10^{-7} (\pm 0.02 \times 10^{-6})$

551

1
2
3 552 **Table 2. Calculated equilibrium dissociation constant (K_D) of the imprinted nanomaterials,**
4 **from data presented in Figures 9 and S9. All experiments were performed under ambient**
5 **553 conditions. Data represents mean \pm S.E.M., n = 3**
6
7
8 555

9
10 556 The interactions of the target protein (BHb) and the corresponding nanoMIPs were calculated
11 557 with K_D values shown to be 2.75 nM and 2.20 nM, for the Batch 1 and Batch 2 nanoMIP,
12 558 respectively. These values show consistency within synthesis of these, with batch-to-batch
13 559 reproducibility. These K_D values are also consistent with our electrochemical method of
14 560 determination (1.03 nM) requiring simple physical (E-layer) entrapment of nanoMIPs on an
15 561 electrode which obviates the need for EDC/NHS coupling reagents. The values are also
16 562 consistent with nanoMIPs, that have been produced using the more popular solid-phase
17 563 synthesis methodology[11]. These studies show nanoMIPs produced *via* the solid-phase
18 564 synthesis to consistently produce binding affinities (K_D values) in the nanomolar range, for
19 565 protein targets such as trypsin and α -casein[40, 43, 44]. With SPR being used as the “gold”
20 566 standard to measure biomolecular interactions[45], the K_D values offered by the nanoMIPs
21 567 produced in this study are shown to be consistent with that of monoclonal antibodies, which
22 568 typically have K_D values within the low nanomolar to sub-nanomolar range[46], thus showing
23 569 these synthetic recognition materials offer excellent recognition to a chosen target[10]. The
24 570 nanomolar binding affinities (K_D values) produced by nanoMIPs is to be expected as
25 571 highlighted by Silva *et al.* due to their small size and large surface area and porosity, leading
26 572 to more consistent and usability synthetic recognition material[47].

27
28 573 Evaluation of the nanoMIPs to discriminate between the target protein (BHb) and other
29 574 proteins was investigated through the challenging of the non-imprinted protein (BSA),
30 575 chosen due to the approximate size and hydrophobic solvent accessible surface areas
31 576 (SASA) and as a representative protein found in complimentary complex matrices. The SPR
32 577 analysis shown in Figures S9 reveals that there is some binding of the BSA to both batches of
33 578 nanoMIP materials, but with vastly reduced affinity, with K_D values of 62.1 and 26.4 μ M, for
34 579 Batch 1 and Batch 2, respectively. This shows that both batches, as expected are selective
35 580 for the template, with K_D values showing an approximate 100-200-fold improvement for the
36 581 target protein (BHb) versus the non-target protein (BSA). This ratio of $K_{D\ BHb}/K_{D\ BSA}$ shows
37 582 that these materials consistently bind more BHb compared with BSA.

38
39 583 Therefore, using our non-solid phase synthesis method with subsequent filtration, we are
40 584 able to produce 2-5 milligram yields of high affinity size selected nanoMIPs in less than 2
41 585 hours. It should be noted though that this synthetic method to produce nanoMIPs requires
42 586 high levels of target protein template (12 mg) to be used per synthesis, which is ultimately
43 587 lost during the washing processes. Whereas this method would not be cost-prohibitive to
44 588 produce MIPs for proteins of high abundance and low-cost, the method does not readily
45 589 lend itself in the case of protein targets which are costly to produce. However, based on our
46 590 investigation of a less harsh (sonication) method used to elute protein (rather than the
47 591 generally accepted chemical denaturation method using SDS/AcOH [18]) we have the
48 592 opportunity to recover non-denatured protein for re-use. This requires further investigation.
49 593 In order to address the need to re-use protein template, other workers have used solid-

1
2
3 594 phase synthesis methods, with target protein attached to glass beads [11] or silane coated
4 595 magnetic beads [48] but these methods are often laborious and time-consuming. In an
5 596 optimised solid phase method[19] we recently reported an unprecedented nanoMIP yield of
6 597 50 mg/mL per day. To complement solid phase methods, we now offer a solution phase
7 598 method to produce and harvest high (2-4 mg/mL) yields of high affinity nanoMIPs within 2
8 599 hours; in a 20 mL reaction volume this equates to 40-80 mg of high affinity material per
9 600 synthesis batch. An additional advantage is the single monomer required here compared
10 601 with other nanoMIP methods which can use as many as 4 monomers in their
11 602 procedures[11].
12
13
14
15
16
17

603

604 **Conclusions**

605 We demonstrate a rapid and simple solution phase synthesis method to produce nanoMIPs
606 with hydrodynamic particle diameters ranging 30 to >800 nm and a total yield of 12 mg/mL
607 in less than 1hr. Using a subsequent 2-5 min process, we are additionally able to size
608 separate nanoMIPs into batches using a sequential range (800 - 100 nm) of polycarbonate
609 membrane filters. NanoMIP rebinding capability and selectivity are a function of particle
610 size. We surmise that excessive filtration is not necessary and a two-stage filtration process
611 using only the 800 nm followed by 400 nm filters is required to harvest high selectivity
612 materials (40-80 mg per 20 mL batch). The nanoMIPs are easily integrated to an
613 electrochemical electrode sensor and we demonstrate nM sensitivity for target (BHb)
614 protein with an acceptable selectivity of 16:1 when compared against a non-target protein.
615 The electrochemical sensor method shows versatility for simple nanoMIP entrapment and
616 sensor application. We also demonstrate for the first time that there is good correlation
617 between the E-layer nanoMIP (electrochemical) method and SPR method to determine K_D .
618

618

619 **Author Contribution**

620 SMR (@UCLan) conceived and directed the research and wrote the manuscript. ANS
621 (@UCLan) performed NanoMIP synthesis, characterisation, and electrochemical studies.
622 SRD (@UCLan) supported with the extrusion method used. MAH (@UCLan) performed AFM
623 studies. NT (@Sheffield) and MS (@OIST) performed SPR measurements. All read and
624 reviewed the manuscript.

625 **Acknowledgements**

626 SMR, ANS, SRD and MAH are grateful to the University of Central Lancashire, Royal Society
627 of Chemistry COVID-19 Action fund (H20-188); RSC Research Enablement Grant (E22-
628 5899202825), the Daiwa Anglo-Japanese Foundation (13094/13916) and The Royal Society
629 (IES\R3\193093) for funding this work. NT and MS would like to thank the University of
630 Sheffield and Engineering and Physical Sciences Research Council (EPSRC) for financial
631 support for this work (EP/V046594/2).
632

632

1
2
3 633 **Data Availability**
4

5 634 All data are available within the article and its Supplementary Information files and from the
6 authors upon request.
7

8 636
9

10 637
11

12 638
13

14 639
15

16 640
17

18 641
19

20 642
21

22 643
23
24
25
26
27
28
29
30
31
32
33
34
35
36
37
38
39
40
41
42
43
44
45
46
47
48
49
50
51
52
53
54
55
56
57
58
59
60

Accepted Manuscript

644 **References**

- 645 [1] Ecker D M, Jones S D and Levine H L 2015 The therapeutic monoclonal antibody market
646 *mAbs* **7** 9-14
- 647 [2] El-Sharif H F, Hawkins D M, Stevenson D and Reddy S M 2014 Determination of protein
648 binding affinities within hydrogel-based molecularly imprinted polymers (HydroMIPs)
649 *Physical Chemistry Chemical Physics* **16** 15483-9
- 650 [3] Boonpangrak S, Whitcombe M J, Prachayasittikul V, Mosbach K and Ye L 2006 Preparation of
651 molecularly imprinted polymers using nitroxide-mediated living radical polymerization
652 *Biosensors and Bioelectronics* **22** 349-54
- 653 [4] El-Sharif H F, Phan Q T and Reddy S M 2014 Enhanced selectivity of hydrogel-based
654 molecularly imprinted polymers (HydroMIPs) following buffer conditioning *Analytica*
655 *Chimica Acta* **809** 155-61
- 656 [5] Ye L, Yu Y and Mosbach K 2001 Towards the development of molecularly imprinted artificial
657 receptors for the screening of estrogenic chemicals *Analyst* **126** 760-5
- 658 [6] Schmidt R H and Haupt K 2005 Molecularly Imprinted Polymer Films with Binding Properties
659 Enhanced by the Reaction-Induced Phase Separation of a Sacrificial Polymeric Porogen
660 *Chemistry of Materials* **17** 1007-16
- 661 [7] Schmidt R H, Mosbach K and Haupt K 2004 A simple method for spin-coating molecularly
662 imprinted polymer films of controlled thickness and porosity *Advanced Materials* **16** 719-22
- 663 [8] Sullivan M, Dennison S, Hayes J and Reddy S 2021 Evaluation of acrylamide-based
664 molecularly imprinted polymer thin-sheets for specific protein capture - a myoglobin model
665 *Biomedical Physics & Engineering Express* **7**
- 666 [9] Sullivan M V, Nanalal S, Dean B E and Turner N W 2024 Molecularly imprinted polymer
667 hydrogel sheets with metalloporphyrin-incorporated molecular recognition sites for protein
668 capture *Talanta* **266** 125083
- 669 [10] Poma A, Guerreiro A, Whitcombe M J, Piletska E V, Turner A P F and Piletsky S A 2013 Solid-
670 Phase Synthesis of Molecularly Imprinted Polymer Nanoparticles with a Reusable Template-
671 "Plastic Antibodies" *Advanced Functional Materials* **23** 2821-7
- 672 [11] Canfarotta F, Poma A, Guerreiro A and Piletsky S 2016 Solid-phase synthesis of molecularly
673 imprinted nanoparticles *Nature Protocols* **11** 443-55
- 674 [12] Sullivan M V, Fletcher C, Armitage R, Blackburn C and Turner N W 2023 A rapid synthesis of
675 molecularly imprinted polymer nanoparticles for the extraction of performance enhancing
676 drugs (PIEDs) *Nanoscale Advances* **5** 5352-60
- 677 [13] Graham S P, El-Sharif H F, Hussain S, Fruengel R, McLean R K, Hawes P C, Sullivan M V and
678 Reddy S M 2019 Evaluation of Molecularly Imprinted Polymers as Synthetic Virus
679 Neutralizing Antibody Mimics *Frontiers in Bioengineering and Biotechnology* **7**
- 680 [14] El Sharif H F, Dennison S R, Tully M, Crossley S, Mwangi W, Bailey D, Graham S P and Reddy S
681 M 2022 Evaluation of electropolymerized molecularly imprinted polymers (E-MIPs) on
682 disposable electrodes for detection of SARS-CoV-2 in saliva *Analytica Chimica Acta* **1206**
683 339777
- 684 [15] Stephen A N, Dennison S R, Holden M A and Reddy S M 2023 Rapid sub-nanomolar protein
685 determination in serum using electropolymerized molecularly imprinted polymers (E-MIPs)
686 *Analyst* **148** 5476-85
- 687 [16] Leibl N, Duma L, Gonzato C and Haupt K 2020 Polydopamine-based molecularly imprinted
688 thin films for electro-chemical sensing of nitro-explosives in aqueous solutions
689 *Bioelectrochemistry* **135** 107541
- 690 [17] Phonklam K, Wannapob R, Sriwimol W, Thavarungkul P and Phairatana T 2020 A novel
691 molecularly imprinted polymer PMB/MWCNTs sensor for highly-sensitive cardiac troponin T
692 detection *Sensors and Actuators B: Chemical* **308** 127630

- 1
2
3 693 [18] Hawkins D M, Stevenson D and Reddy S M 2005 Investigation of protein imprinting in
4 694 hydrogel-based molecularly imprinted polymers (HydroMIPs) *Analytica Chimica Acta* **542** 61-
5 695 5
6 696 [19] Reddy S M, Stephen A N, Holden M A, Stockburn W J and Dennison S 2024 Magnetic
7 697 Nanoparticle Facilitated Rapid Mass Production of High Affinity Polymeric Materials
8 698 (nanoMIPs) for Protein Recognition and Biosensing *Biomaterials Science*
9 699 [20] Sullivan M V, Dennison S R, Hayes J M and Reddy S M 2021 Evaluation of acrylamide-based
10 700 molecularly imprinted polymer thin-sheets for specific protein capture—a myoglobin model
11 701 *Biomedical Physics & Engineering Express* **7** 045025
12 702 [21] Tai D-F, Jhang M-H, Chen G-Y, Wang S-C, Lu K-H, Lee Y-D and Liu H-T 2010 Epitope-Cavities
13 703 Generated by Molecularly Imprinted Films Measure the Coincident Response to Anthrax
14 704 Protective Antigen and Its Segments *Analytical Chemistry* **82** 2290-3
15 705 [22] Kan X, Xing Z, Zhu A, Zhao Z, Xu G, Li C and Zhou H 2012 Molecularly imprinted polymers
16 706 based electrochemical sensor for bovine hemoglobin recognition *Sensors and Actuators B:*
17 707 *Chemical* **168** 395-401
18 708 [23] Hix-Janssens T, Davies J R, Turner N W, Sellergren B and Sullivan M V 2024 Molecularly
19 709 imprinted nanogels as synthetic recognition materials for the ultrasensitive detection of
20 710 periodontal disease biomarkers *Analytical and Bioanalytical Chemistry*
21 711 [24] McClements J, Bar L, Singla P, Canfarotta F, Thomson A, Czulak J, Johnson R E, Crapnell R D,
22 712 Banks C E, Payne B, Seyedin S, Losada-Pérez P and Peeters M 2022 Molecularly Imprinted
23 713 Polymer Nanoparticles Enable Rapid, Reliable, and Robust Point-of-Care Thermal Detection
24 714 of SARS-CoV-2 *ACS Sensors* **7** 1122-31
25 715 [25] Garcia Cruz A, Haq I, Cowen T, Di Masi S, Trivedi S, Alanazi K, Piletska E, Mujahid A and
26 716 Piletsky S A 2020 Design and fabrication of a smart sensor using in silico epitope mapping
27 717 and electro-responsive imprinted polymer nanoparticles for determination of insulin levels
28 718 in human plasma *Biosensors and Bioelectronics* **169** 112536
29 719 [26] Cáceres C, Canfarotta F, Chianella I, Pereira E, Moczko E, Esen C, Guerreiro A, Piletska E,
30 720 Whitcombe M J and Piletsky S A 2016 Does size matter? Study of performance of pseudo-
31 721 ELISAs based on molecularly imprinted polymer nanoparticles prepared for analytes of
32 722 different sizes *Analyst* **141** 1405-12
33 723 [27] Yucel N, Gulen H and Cakir Hatir P 2022 Molecularly imprinted polymer nanoparticles for the
34 724 recognition of ellagic acid *Journal of Applied Polymer Science* **139** e52952
35 725 [28] Shen X, Huang C, Shinde S, Jagadeesan K K, Ekström S, Fritz E and Sellergren B 2016 Catalytic
36 726 Formation of Disulfide Bonds in Peptides by Molecularly Imprinted Microgels at Oil/Water
37 727 Interfaces *ACS Applied Materials & Interfaces* **8** 30484-91
38 728 [29] Heller G T, Mercer-Smith A R and Johal M S 2015 *Protein-Protein Interactions: Methods and*
39 729 *Applications*, ed C L Meyerkord and H Fu (New York, NY: Springer New York) pp 153-64
40 730 [30] Tsai T-C, Liu C-W, Wu Y-C, Ondevilla N A P, Osawa M and Chang H-C 2019 In situ study of
41 731 EDC/NHS immobilization on gold surface based on attenuated total reflection surface-
42 732 enhanced infrared absorption spectroscopy (ATR-SEIRAS) *Colloids and Surfaces B:*
43 733 *Biointerfaces* **175** 300-5
44 734 [31] Erol K, Hasabnis G and Altintas Z 2023 A Novel NanoMIP-SPR Sensor for the Point-of-Care
45 735 Diagnosis of Breast Cancer *Micromachines (Basel)* **14**
46 736 [32] Fischer M J E 2010 *Surface Plasmon Resonance: Methods and Protocols*, ed N J Mol and M J E
47 737 Fischer (Totowa, NJ: Humana Press) pp 55-73
48 738 [33] Hejazi S M, Erfan M and Mortazavi S A 2013 Precipitation Reaction of SDS and Potassium
49 739 Salts in Flocculation of a Micronized Megestrol Acetate Suspension *Iran J Pharm Res* **12** 239-
50 740 46
51 741 [34] Sengel S B and Sahiner N 2019 Synthesis and characterization of poly(N-(2-mercaptoethyl)
52 742 acrylamide) microgel for biomedical applications *Polymers for Advanced Technologies* **30**
53 743 2109-21
54
55
56
57
58
59
60

- 1
2
3 744 [35] Acciaro R, Gilányi T and Varga I 2011 Preparation of Monodisperse Poly(N-
4 745 isopropylacrylamide) Microgel Particles with Homogenous Cross-Link Density Distribution
5 746 *Langmuir* **27** 7917-25
- 6 747 [36] Patton J N and Palmer A F 2006 Physical Properties of Hemoglobin–Poly(acrylamide)
7 748 Hydrogel-Based Oxygen Carriers: Effect of Reaction pH *Langmuir* **22** 2212-21
- 8 749 [37] Neises B and Steglich W 1978 Simple Method for the Esterification of Carboxylic Acids
9 750 *Angewandte Chemie International Edition in English* **17** 522-4
- 10 751 [38] Tsakos M, Schaffert E S, Clement L L, Villadsen N L and Poulsen T B 2015 Ester coupling
11 752 reactions – an enduring challenge in the chemical synthesis of bioactive natural products
12 753 *Natural Product Reports* **32** 605-32
- 13 754 [39] Sullivan M V, Henderson A, Hand R A and Turner N W 2022 A molecularly imprinted polymer
14 755 nanoparticle-based surface plasmon resonance sensor platform for antibiotic detection in
15 756 river water and milk *Analytical and Bioanalytical Chemistry* **414** 3687-96
- 16 757 [40] Cáceres C, Moczko E, Basozabal I, Guerreiro A and Piletsky S 2021 Molecularly Imprinted
17 758 Nanoparticles (NanoMIPs) Selective for Proteins: Optimization of a Protocol for Solid-Phase
18 759 Synthesis Using Automatic Chemical Reactor. In: *Polymers*,
- 19 760 [41] Abbas A, Linman M J and Cheng Q 2011 Sensitivity comparison of surface plasmon
20 761 resonance and plasmon-waveguide resonance biosensors *Sensors and Actuators B: Chemical*
21 762 **156** 169-75
- 22 763 [42] Chabot V, Miron Y, Grandbois M and Charette P G 2012 Long range surface plasmon
23 764 resonance for increased sensitivity in living cell biosensing through greater probing depth
24 765 *Sensors and Actuators B: Chemical* **174** 94-101
- 25 766 [43] Sullivan M V, Clay O, Moazami M P, Watts J K and Turner N W 2021 Hybrid Aptamer-
26 767 Molecularly Imprinted Polymer (aptaMIP) Nanoparticles from Protein Recognition—A
27 768 Trypsin Model *Macromolecular Bioscience* **21** 2100002
- 28 769 [44] Ashley J, Shukor Y, D'Aurelio R, Trinh L, Rodgers T L, Temblay J, Pleasants M and Tothill I E
29 770 2018 Synthesis of Molecularly Imprinted Polymer Nanoparticles for α -Casein Detection Using
30 771 Surface Plasmon Resonance as a Milk Allergen Sensor *ACS Sensors* **3** 418-24
- 31 772 [45] Khan S H, Farkas K, Kumar R and Ling J 2012 A versatile method to measure the binding to
32 773 basic proteins by surface plasmon resonance *Analytical Biochemistry* **421** 385-90
- 33 774 [46] Friguet B, Chaffotte A F, Djavadi-Ohanian L and Goldberg M E 1985 Measurements of the
34 775 true affinity constant in solution of antigen-antibody complexes by enzyme-linked
35 776 immunosorbent assay *Journal of Immunological Methods* **77** 305-19
- 36 777 [47] Silva A T, Figueiredo R, Azenha M, Jorge P A S, Pereira C M and Ribeiro J A 2023 Imprinted
37 778 Hydrogel Nanoparticles for Protein Biosensing: A Review *ACS Sensors* **8** 2898-920
- 38 779 [48] Mahajan R, Rouhi M, Shinde S, Bedwell T, Incel A, Mavliutova L, Piletsky S, Nicholls I A and
39 780 Sellergren B 2019 Highly Efficient Synthesis and Assay of Protein-Imprinted Nanogels by
40 781 Using Magnetic Templates *Angewandte Chemie International Edition* **58** 727-30

782